Journal of Alloys and Compounds 504 (2010) 205–210

Contents lists available at ScienceDirect

Journal of Alloys and Compounds

journal homepage: www.elsevier.com/locate/jallcom

Al–Fe hypoeutectic alloys directionally solidified under steady-state and unsteady-state conditions

P.R. Goulart[a], J.E. Spinelli[b], N. Cheung[a,c], N. Mangelinck-Nöel[d], A. Garcia[a,*]

[a] Department of Materials Engineering, University of Campinas – UNICAMP, PO Box 6122, 13083-860, Campinas, SP, Brazil
[b] Department of Materials Engineering, Federal University of Rio Grande do Norte – UFRN, PO Box 1524, 59072-970, Lagoa Nova Campus, Natal, RN, Brazil
[c] Federal Institute of Education, Science and Technology of São Paulo – IFSP, 13872-55, São João da Boa Vista, SP, Brazil
[d] IM2NP, UMR 6137, University Paul Cézanne Aix-Marseille III, Faculté de Saint-Jérome, Service 142, 13397 Marseille Cedex 20, France

ARTICLE INFO

Article history:
Received 7 April 2010
Received in revised form 8 May 2010
Accepted 14 May 2010
Available online 27 May 2010

Keywords:
Metals and alloys
Intermetallics
Microstructure
Thermal analysis

ABSTRACT

The aim of this work is to evaluate the cellular growth, the nature of Al–Fe intermetallic particles and the eutectic arrangement of Al–Fe hypoeutectic samples solidified at growth rates ranging from 0.05 to 2.5 mm/s. The samples grown at higher solidification velocities were obtained using a water-cooled directional solidification apparatus. A Bridgman-type furnace was used to grow samples in the lower range of solidification velocities and an air-cooled mold was used to generate experimental values in between those obtained by the other two techniques of directional solidification. All casting assemblies were set to support upward directional solidification. Based on the present results, a single experimental power law seems to be enough to fit all experimental values of cell spacing as a function of cooling rate. The wide range of solidification thermal parameters used in the present study was chosen due to the diversity of foundry processes used for the manufacture of Al–Fe alloys components. For instance, low solidification velocities are typical of sand casting processes while high velocities are typical of direct-chill (DC) castings. In order to investigate the nature of the Al–Fe intermetallics, these particles were extracted from the aluminum-rich matrix by using a dissolution technique. Such phases were then investigated by SEM-EDAX microscopy and X-ray diffraction (XRD). It was found that Al_3Fe is the predominant intermetallic phase in the Bridgman-grown samples and Al_6Fe prevails in the samples grown in the water-cooled solidification apparatus.

1. Introduction

A widely accepted method for achieving controlled solidification conditions is the directional solidification in Bridgman-type furnaces. These systems are built to permit the independent control of both the thermal gradient (G) and growth rate (v). Very low growth rates are possible to be imposed even when large temperature gradients are set. A number of studies have been developed in such systems with a view to understanding the dependence of the as-solidified microstructures of binary alloys on the solidification thermal parameters [1–14]. While most investigations have focused on the final steady-state of solidification processes the knowledge gained from these experiments is limited because many phenomena can only be explained by taking into account dynamical processes, such as the continuous arrangement of the solidification patterns. Unsteady-state solidification experimental studies on binary [15–22] and ternary [23] alloys have been accomplished by water-cooled molds with unidirectional heat extraction. Such conditions are very close to those found in many industrial foundry processes.

Most of the unidirectional solidification studies on Al–Fe alloys existing in literature have been carried out with a view to characterizing microstructural aspects under steady-state solidification conditions. Allen et al. [24] have written a very comprehensive review of such studies. These authors have analyzed Al–Fe alloys in the range of 0.5–1.5 wt%Fe and observed the coexistence of Al_3Fe (equilibrium phase) and Al_6Fe (metastable phase) over the solidification velocity range of 0.2–0.6 mm s^{-1}, which was shown to be independent of Fe alloying content. They have also observed that when the solidification velocity exceeded 0.6 mm s^{-1}, only Al_6Fe intermetallic particles could be detected. On the other hand, Goulart et al. [25] found that Al_6Fe prevails for growth rates higher than 0.7 mm s^{-1} after performing experiments with hypoeutectic Al–Fe alloys under unsteady-state solidification conditions.

Hunt [1] and Kurz and Fisher [2,3] proposed detailed theoretical models to characterize cells and primary dendrite spacings during steady-state growth conditions, which are based only on diffusive transport. Hunt has based his model on two major assumptions:

* Corresponding author. Tel.: +55 1935213320; fax: +55 1932893722.
E-mail address: amaurig@fem.unicamp.br (A. Garcia).

0925-8388/$ – see front matter © 2010 Elsevier B.V. All rights reserved.
doi:10.1016/j.jallcom.2010.05.089

a dendrite or cell profile approximated by a smooth steady-state shape even when dendrite arms have been formed and constant temperature and liquid composition in the direction normal to the primary dendritic growth direction. Kurz and Fisher have assumed that the overall morphology of the dendrite (tip and trunk) can be approximated by an ellipsoid. They consider that this shape has the advantage over the paraboloid, that a parabolic-like form exists at the tip, while the lower part of the ellipsoid better represents the real dendrite.

The equations representing these two theories can be expressed, respectively by:

$$\lambda_1 = 2.83[\Gamma m_L C_0(1-k_0)D]^{1/4} G_L^{-1/2} V_L^{-1/4}$$

(Hunt, cellular/dendritic) (1)

$$\lambda_1 = 4.3\left(\frac{\Gamma \Delta T D}{k_0}\right)^{1/4} G_L^{-1/2} V_L^{-1/4}$$

(Kurz and Fisher, cellular/dendritic), (2)

where λ_1 is the cellular spacing, Γ is the Gibbs–Thomson coefficient, m_L is the liquidus line slope, C_0 is the alloy composition, k_0 is the solute partition coefficient, D is the liquid solute diffusivity, ΔT is the difference between the liquidus and solidus equilibrium temperatures, V_L is the cell tip growth rate (in the case of the Bridgman technique the pulling rate, v, must be considered) and G_L is the temperature gradient ahead the cell tip.

A recent study developed an analysis of the "as-solidified" microstructure of Al–Fe hypoeutectic alloys, grown under unsteady-state heat flow conditions [20,21]. Cellular structures prevailed in all examined alloys, whose compositions were Al 0.5, 1.0 and 1.5 wt% Fe. The cell spacing (λ_1) was found to be independent on the alloy Fe content and experimental power laws which fitted the experimental points with exponents −0.55 and −1.1 for the cooling rate and tip growth rate, respectively, have been proposed. Steady-state growth models like those proposed by Hunt [1] and Kurz and Fisher [2] have been checked against the experimental λ_1 values. The experimental scatter lied below the calculations performed with the Kurz–Fisher model, and tended to approach Hunt's model reasonably well for any alloy experimentally examined [21]. The lowest solidification velocity obtained by these authors was of about 0.6 mm/s. Consequently, the use of a Bridgman technique could be very useful in order to check the application of the aforementioned experimental power laws under very low growth rate conditions. As stated by Allen et al. [24], at very low velocities under steady-state solidification, Al_3Fe intermetallic particles are expected to be predominant.

Experimental λ_1 results obtained under steady-state conditions can also be valuable to check the applicability of the aforementioned steady-state cellular growth models for Al–Fe hypoeutectic alloys. Steady-state and unsteady-state growth regimes can be considered as complementary solidification techniques due to the possibility of scanning a larger range of cooling rates, solidification velocities and consequently of cell spacings. The present work focuses on the dependence of the cell spacing on the solidification thermal parameters in both the steady-state and unsteady-state regimes of solidification for hypoeutectic Al–Fe alloys. The experimental dependences of λ_1 on the cooling rate and tip growth rate are checked taking into account a large range of solidification thermal parameters. The experimental λ_1 data obtained by the Bridgman technique are compared with the theoretical predictions of models for cellular growth under steady-state conditions. A matrix dissolution technique associated with XRD analysis was carried out with a view to checking the nature of the Al–Fe intermetallic particles for growth rates lower than 300 μm/s.

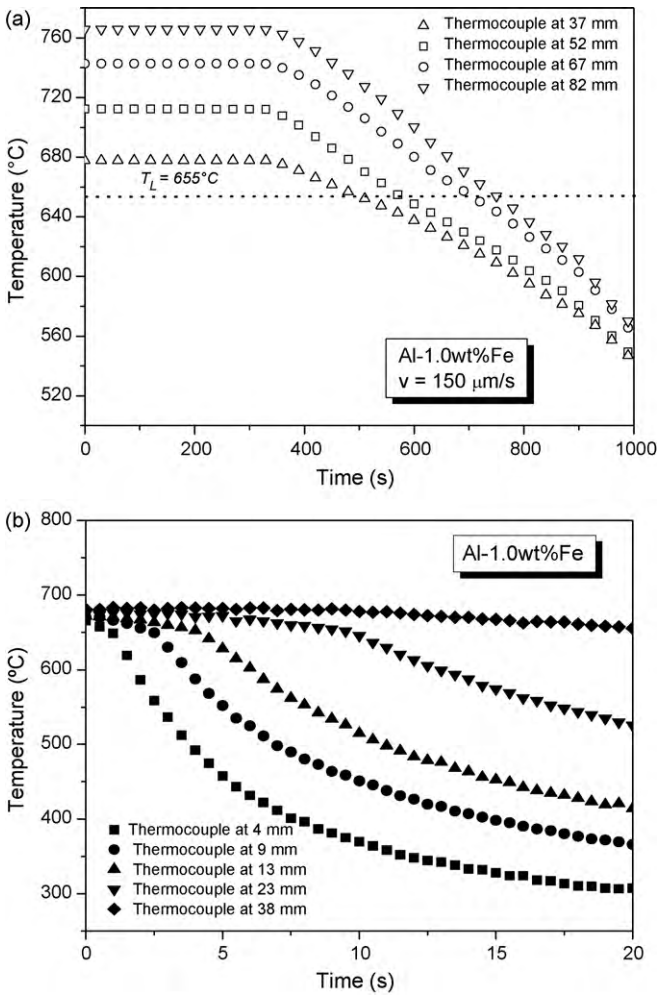

Fig. 1. Experimental cooling curves for the Al–1.0 wt%Fe alloy samples (a) in the Bridgman apparatus and (b) in the water-cooled directional solidification system.

2. Experimental procedure

Directional solidification experiments with hypoeutectic Al–Fe alloys (0.5, 1.0 and 1.5 wt% Fe) were carried out in three different solidification experimental set-ups. Very low solidification velocities were imposed by a Bridgman furnace while higher velocities were obtained by a water-cooled solidification apparatus, which is characterized by unsteady-state heat flow conditions. Specific information about both systems can be found in previous articles [20,26]. In order to permit the effect of the range of cooling rates between those of the Bridgman and the water-cooled set-ups in the resulting microstructure to be examined, air-cooled directional solidification experiments were also conducted.

In the Bridgman furnace, a temperature gradient (G) of 1.5 K/mm was kept constant for all the experiments. The samples are initially located in the hot zone where they are liquid. Then, they are pulled down towards the lower and colder zone where they start to solidify. The experiments were performed at three different pulling rates (v): 50, 150 and 300 μm/s. Before pulling, a stabilization period of 90 min was set to homogenize the temperature in the melt. A boron nitride crucible was used having an internal diameter of 9 mm and a height of 110 mm. This crucible was closed with a bottom plug. Four type-K thermocouples were placed along the outside wall of the crucible at 37, 52, 67 and 82 mm from the bottom of the sample. These thermocouples were connected to a datalogger in order to permit temperature data to be read and recorded. The acquisition rate was set at 1 measurement per second.

In the unsteady-state solidification system, heat is directionally extracted only through a water-cooled bottom made of low carbon steel (SAE 1020), promoting vertical upward directional solidification. A stainless steel split mold was used having an internal diameter of 60 mm, a height of 157 mm and a wall thickness of 5 mm. The inner surface of mold side walls was covered with a 1 mm thick layer of insulating alumina to minimize radial heat losses. The bottom part of the mold was closed with a thin (3 mm thick) carbon steel sheet.

The initial melt temperatures (T_p) were standardized at 10 °C above the *liquidus* temperature (T_{Liq}) for the unsteady-state experiments. Continuous temperature measurements in the casting were monitored during solidification via the output of

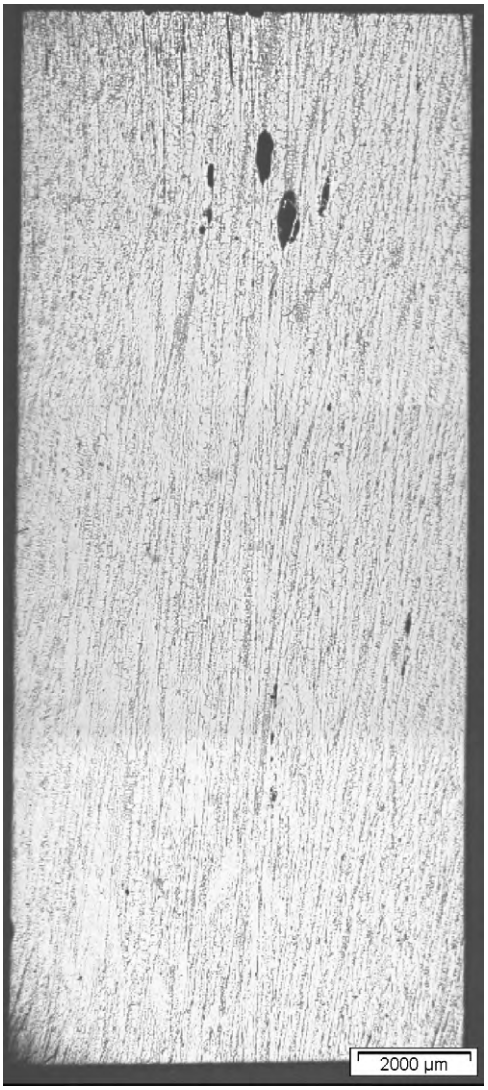

Fig. 2. Directionally solidified macrostructure of an Al–1.0 wt%Fe Bridgman sample (G = 1.5 K/mm and v = 150 μm/s).

a bank of fine type-K thermocouples (made from 0.2 mm diameter wire), sheathed in 1.6 mm diameter stainless steel tubes and positioned at 4, 9, 13, 17, 23, 38, 53, 68 and 88 mm from the heat-extracting surface at the bottom. The thermocouples were calibrated at the melting point of aluminum exhibiting fluctuations of about 1 °C. The thermocouples were connected by coaxial cables to a data logger interfaced

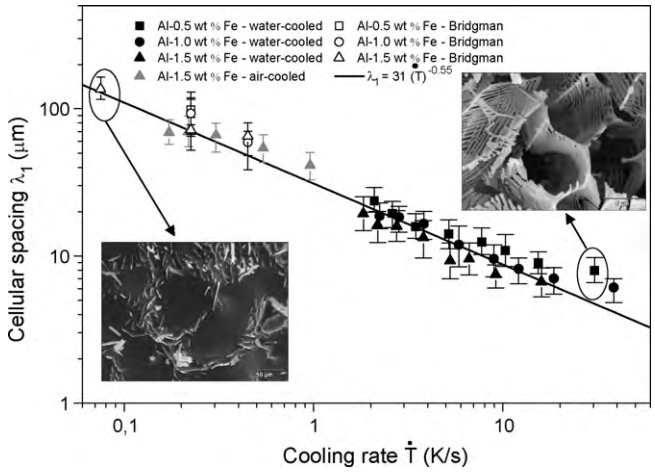

Fig. 3. Cellular spacing as a function of the cooling rate.

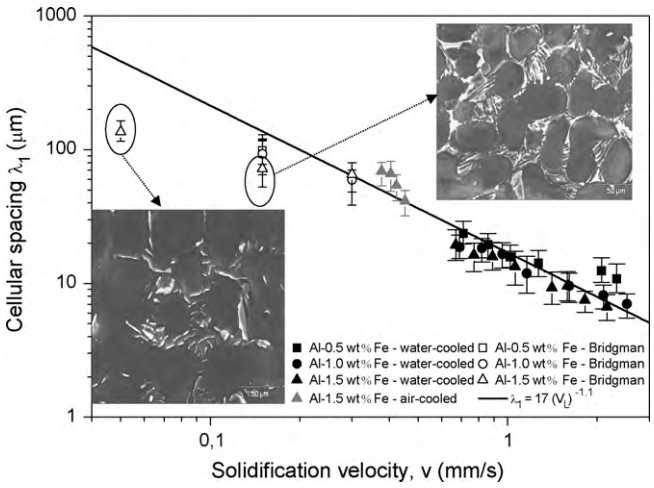

Fig. 4. Cellular spacing as a function of the tip growth rate.

with a computer, and the temperature data, read at intervals of 0.1 s, were acquired automatically.

Each cylindrical ingot was subsequently sectioned along its vertical axis, ground and etched with an acid solution to reveal the macrostructure (Poulton's reagent: 5 mL H_2O; 5 mL HF – 48%; 30 mL HNO_3; 60 mL HCl). Selected transverse (perpendicular to the growth direction) and longitudinal sections of the directionally solidified castings at different positions from the metal/mold interface were electropolished and etched (a solution of 0.5% HF in water) for metallography. An image processing system was used to measure the cellular spacing, λ_1 (about 40 independent readings for each selected position, with the average taken to be the local spacing) and its distribution range. The method used for measuring the cellular spacing on the transverse section (perpendicular to the growth direction) was the triangle method [12,13]. The interphase eutectic spacing was measured in the SEM images of the Al–1.5 wt%Fe alloy castings by a linear intercept method [27,28].

Based on the method for quantitative analysis of intermetallics of aluminum alloys proposed by Simensen et al. [29,30], a glass apparatus [25] was used to dissolve the Al-rich matrix and the eutectic aluminum-phase so that only Al–Fe intermetallic particles remained. The samples of about 3–5 g were partially dissolved in distilled 1-butanol under argon atmosphere. After dissolution, the butanol and the aluminum butoxides were conducted through a Teflon filter with a pore size of 0.45 μm. The undissolved intermetallics retained by the Teflon filter were identified and analyzed by X-ray diffraction and scanning electron microscopy (SEM) with energy-dispersive X-ray analyzer. In order to achieve a better visualization of the SEM microstructures, the samples were ever rotated in about 30°.

The extracted intermetallics obtained from the solidified samples were characterized by XRD with a Rigaku DMAX 2200 diffractometer (40 kV, 30 mA), in

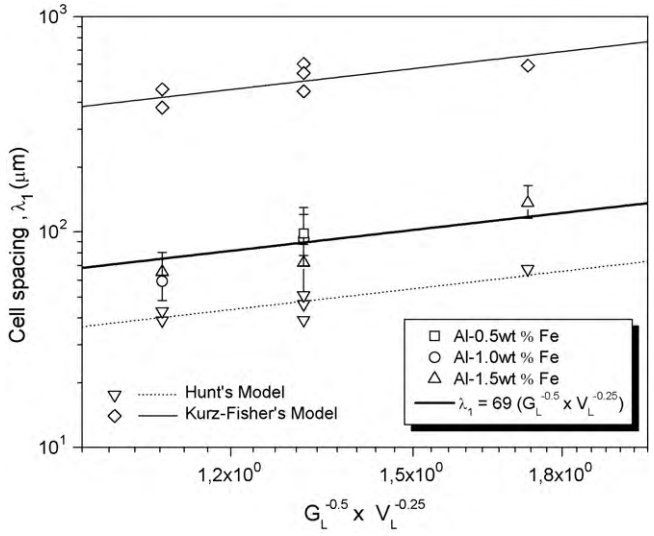

Fig. 5. Comparison of experimental (steady-state) and theoretical (steady-state) cellular spacings for unidirectionally solidified Al–0.5 wt%Fe, Al–1.0 wt%Fe and Al–1.5 wt%Fe alloys.

Bragg–Brentano reflection geometry with Cu Kα radiation (λ = 1.5418 Å). The data were obtained between 10° and 70° 2θ in steps of 0.1° with counting time of 3 s.

3. Results and discussion

Fig. 1a shows a typical set of cooling curves recorded along the Al–1.0 wt%Fe sample during directional solidification in the Bridgman furnace. The pulling rate in this case was 150 μm/s. The readings of the two first thermocouples were used to determine the thermal gradient (G). All metallographic procedures have been conducted in the first 50 mm of the Bridgman samples. The cooling rate ($\dot{T}$) corresponding to the Bridgman samples was determined from the experimental values of pulling rate (v) and temperature gradient (G): ($\dot{T} = Gv$). While experimental measurements of cooling rates during solidification in the Bridgman process provide critical thermal information, it is typically acquired at only a few key locations. Nonetheless, this is still one of the best experimental tools for probing actual solidification conditions. [31].

Fig. 1b shows a typical example of experimental cooling curves obtained for the Al–1.0 wt%Fe alloy during directional solidification under unsteady-state conditions in a water-cooled solidification set-up. In the case of unsteady-state solidification, the thermocouples readings have also been used to generate a plot of position from the metal/mold interface as a function of time corresponding to the *liquidus* front passing by each thermocouple. A curve fitting technique on these experimental points has generated a power function of position as a function of time. The derivative of this function with respect to time yields values for tip growth rate (V_L). The data acquisition system, in which temperature readings are collected at a frequency of 0.1 s, permits accurate determination of the slope

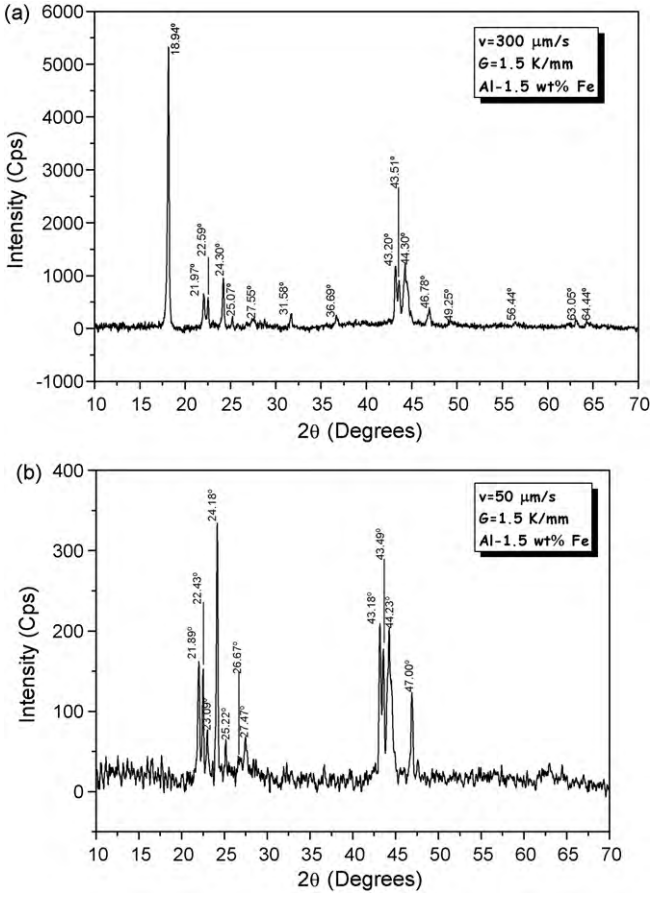

Fig. 6. X-ray diffractograms of Bridgman-grown Al–1.5 wt%Fe alloy samples: (a) 300 μm/s; (b) 50 μm/s.

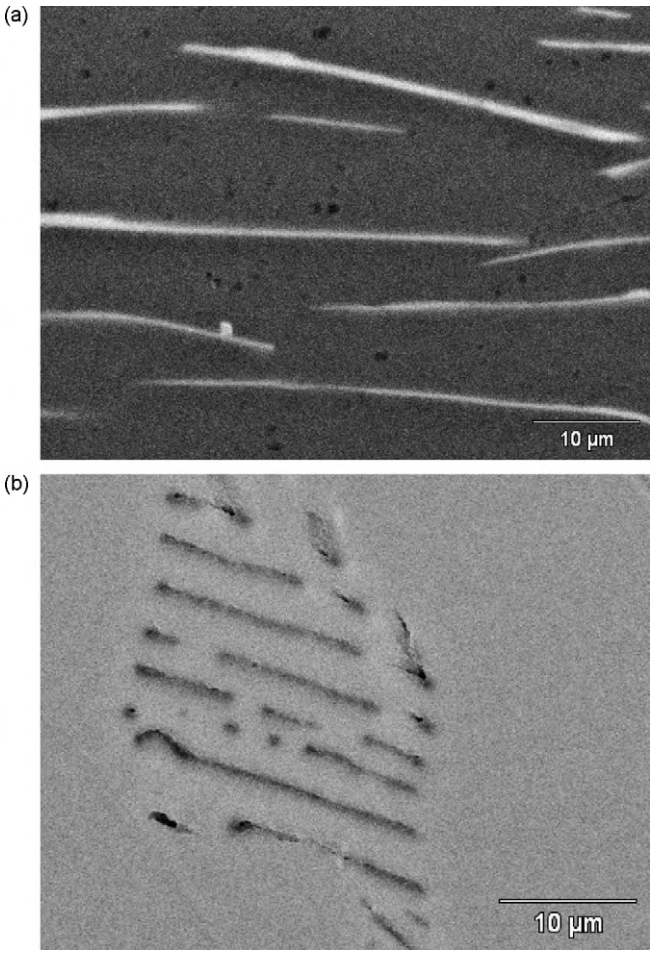

Fig. 7. Eutectic microstructure in the intercellular region for a directionally solidified Al–1.5 wt%Fe alloy at a constant temperature gradient (1.5 K/mm): (a) 50 μm/s; (b) 300 μm/s.

of the experimental cooling curves. The cooling rate ($\dot{T}$) was determined by considering the thermal data recorded immediately after the passing of the liquidus front by each thermocouple.

Recent studies [21,22] detail the cellular growth during unsteady-state directional solidification of hypoeutectic Al–Fe alloys and hypomonotectic Al-Bi alloys. For all the examined alloys, columnar grains prevailed along the entire casting length. The Bridgman Al–Fe samples have also entire columnar macrostructures, as the typical example shown in Fig. 2 for an Al–1.0 wt%Fe sample grown at G = 1.5 K/mm and v = 150 μm/s.

Fig. 3 shows the evolution of cell spacing (λ_1) as a function of cooling rate ($\dot{T}$) as well as typical SEM microstructures observed in the present study. A single −0.55 experimental power law characterizes the λ_1 evolution with cooling rate even if very low solidification velocities are considered as those obtained in the Bridgman apparatus. It is important to remark that the cell spacing has not been affected by the alloy solute content.

The unsteady-state solidification apparatus was also adapted with an air-cooled mold. Then, an additional experiment with the Al–1.5 wt%Fe alloy was carried out and the resulting experimental λ_1 values have been included in the experimental spectrum (gray triangles in Fig. 3).

The microstructures shown in Fig. 3 give an overview of the intermetallic network along the transverse sections of Al–Fe alloys, after the dissolution of the Al-rich phase in distilled 1-butanol. An arrangement of cells has prevailed in all examined samples solidified either under steady-state or unsteady-state conditions. While

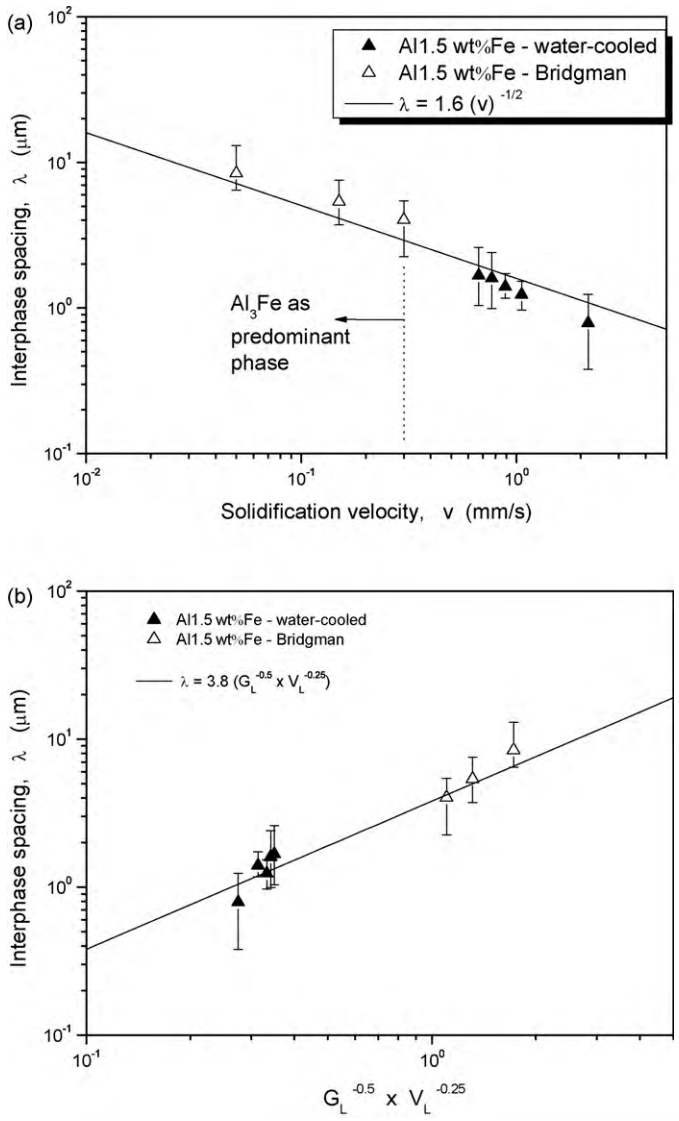

Fig. 8. Eutectic interphase spacing for an Al–1.5 wt%Fe alloy as a function of (a) solidification velocity and (b) $G_L^{-1/2} \times V_L^{-1/4}$.

the Al_6Fe rod-like intermetallics are connected to the high cooling rates range during solidification, Al_3Fe plate-like particles prevail in the lower range of cooling rate values.

Fig. 4 shows the evolution of λ_1 as a function of tip growth rate. Typical SEM images of a partially dissolved Al–1.5 wt%Fe alloy sample are also included in Fig. 4 emphasizing the prevalence of the Al_3Fe plate-like phase in the Bridgman-grown samples. The experimental law which fits the experimental scatter generated under unsteady-state solidification conditions does not represent the higher λ_1 experimental values obtained at low solidification velocities in the Bridgman furnace. Thi et al. [26] performed steady-state solidification experiments with an Al–1.5 wt%Ni alloy. They stated that the solute boundary layer adjacent to the tips is swept by the fluid flow driven by the radial temperature gradient. A convex shape of the isotherms and a narrow front depression at the crucible wall were observed, which results on solute accumulation at the crucible periphery. The effects of this buoyancy-driven convection decrease with increasing solidification velocity. Thus, it seems that convection action during solidification of the Al–1.5 wt%Fe alloy at 50 μm/s could be effective enough to affect the solute layer immediately ahead the solidification front. In this case, the advance of the liquidus isotherm may be accelerated decreasing λ_1.

Fig. 5 shows a comparison between the steady-state experimental λ_1 scatter and the theoretical predictions furnished by the main cellular growth models existing in the literature for steady-state conditions. The Bridgman λ_1 results are in disagreement with the steady-state predictions of both Hunt and Kurz–Fisher models. However, it is important to remark that the slopes of the experimental and theoretical curves are the same. The thermophysical properties used in the calculations are those reported in a recent article [20].

Some XRD patterns of Al–Fe Bridgman samples are shown in Fig. 6. There are many peaks characterizing the Al_3Fe phase, which seems to be the dominant intermetallic phase considering pulling rates lower than 300 μm/s for hypoeutectic Al–Fe alloys.

Some typical SEM images of the intercellular region for a directionally solidified Al–1.5 wt%Fe alloy are shown in Fig. 7a and b. These transverse microstructures consist of a eutectic mixture of Al–Fe intermetallic particles embedded in the Al-rich phase. The eutectic interphase spacing was determined from these microstructures. Fig. 8a shows the average experimental values of interphase spacing and its distribution range as a function of growth rate. Points are experimental results and the line represents a single empirical fit to the experimental points which follows the classical growth law for eutectics: $(\lambda^2 v = C)$ [2]. The experimental law seems to be appropriated for both steady-state and unsteady-state results no matter if the prevailing intermetallics is the Al_3Fe (equilibrium phase) or Al_6Fe.

Fig. 8b shows the dependence of the interphase spacing on $G \times v$ for the Al–1.5 wt%Fe alloy. The main theoretical models for cellular/dendritic growth, which were developed for steady-state conditions, propose specific exponents to be used in this kind of correlation ($-1/2$ for G and $-1/4$ for v) [1–5]. In the present experimental investigation, which was conducted under conditions of unsteady and steady-state growth, the exponents $-1/2$ for G and $-1/4$ for v were found to be appropriate for the eutectic growth of the Al–1.5 wt%Fe alloy, as shown in Fig. 8b.

4. Conclusions

The following major conclusions can be drawn from the present experimental investigation:

(a) A single $\lambda_1 = 31(\dot{T})^{-0.55}$ experimental power law represents the whole λ_1 experimental scatter, including the Bridgman low range of growth rates.
(b) The presence of Al_3Fe plate-like intermetallic particles has been detected in the Bridgman samples while Al_6Fe rod-like intermetallics were found to be connected to the samples which were grown at higher cooling rates. The experimental interdependence of λ_1 on the cooling rate was shown not to be affected by the nature of the intermetallic phase.
(c) Despite the similar slopes of the experimental and theoretical curves of λ_1 as a function of $G^{-1/2} \times v^{-1/4}$, both stationary predictions of Hunt and Kurz–Fisher models have not fitted the λ_1 experimental scatter obtained during steady-state solidification.
(d) The interphase spacing of the eutectic mixture was shown to comply with the following experimental laws in the entire range of steady-state and unsteady-state solidification thermal parameters: $\lambda = 1.6(v)^{-1/2}$ and $\lambda = 3.8G^{-1/2} \times v^{-1/4}$.

Acknowledgements

The authors acknowledge the financial support provided by FAPESP (The Scientific Research Foundation of the State of São Paulo, Brazil), CNPq (The Brazilian Research Council) and FAEPEX –

UNICAMP. This study has also been funded by the ARCUS Program (French Ministry of Foreign Affairs, Région Provence-Alpes-Cote d'Azur and Brazil) and FAPERN (The Scientific Research Foundation of the State of Rio Grande do Norte, Brazil).

References

[1] J.D. Hunt, International Conference on Solidification and Casting of Metals, The Metals Society, London, 1979.
[2] W. Kurz, J.D. Fisher, Acta Metall. 29 (1981) 11–20.
[3] W. Kurz, J.D. Fisher, Fundamentals of Solidification, Trans Tech Public., Switzerland, 1992.
[4] R. Trivedi, Metall. Mater. Trans. A 15A (1984) 977–982.
[5] R. Trivedi, W. Kurz, Int. Mater. Rev. 39 (1994) 49–74.
[6] D. Bouchard, J.S. Kirkaldy, Metall. Mater. Trans. B 27B (1996) 101–113.
[7] D. Bouchard, J.S. Kirkaldy, Metall. Mater. Trans. B 28B (1997) 651–663.
[8] J.D. Hunt, S.Z. Lu, Metall. Mater. Trans. A 27A (1996) 611–623.
[9] V. Laxmanan, Scripta Mater. 38 (1998) 1289–1297.
[10] X. Lin, W.D. Huang, J. Feng, T. Li, Y. Zhou, Acta Mater. 47 (1999) 3271–3280.
[11] J. Feng, W.D. Huang, X. Lin, Q.Y. Pan, T. Li, Y.H. Zhou, J. Cryst. Growth 197 (1999) 393–395.
[12] E. Çardili, M. Gündüz, J. Mater. Sci. 35 (2000) 3837–3848.
[13] M. Gündüz, E. Çardili, Mater. Sci. Eng. A 327 (2002) 167–185.
[14] M. Gündüz, H. Kaya, E. Çardili, N. Marasli, K. Keslioglu, B. Saatçi, J. Alloys Compd. 439 (2007) 114–127.
[15] J.E. Spinelli, K.S. Cruz, M.V. Canté, A. Garcia, Phil. Mag. Lett. 89 (2009) 779–786.
[16] D.M. Rosa, J.E. Spinelli, I.L. Ferreira, A. Garcia, Metall. Mater. Trans. A 39A (2008) 2161–2174.
[17] J.E. Spinelli, D.M. Rosa, I.L. Ferreira, A. Garcia, Mater. Sci. Eng. A 383 (2004) 271–282.
[18] M.V. Canté, J.E. Spinelli, I.L. Ferreira, N. Cheung, A. Garcia, Metall. Mater. Trans. A 39A (2008) 1712–1726.
[19] D.M. Rosa, J.E. Spinelli, I.L. Ferreira, A. Garcia, J. Alloys Compd. 422 (2006) 227–238.
[20] P.R. Goulart, K.S. Cruz, J.E. Spinelli, I.L. Ferreira, N. Cheung, A. Garcia, J. Alloys Compd. 470 (2009) 589–599.
[21] P.R. Goulart, K.S. Cruz, J.E. Spinelli, I.L. Ferreira, N. Cheung, A. Garcia, J. Alloys Compd. 487 (2009) 791–793.
[22] A.P. Silva, J.E. Spinelli, A. Garcia, J. Alloys Compd. 480 (2009) 485–493.
[23] I.L. Ferreira, D.J. Moutinho, L.G. Gomes, O.L. Rocha, A. Garcia, Phil. Mag. Lett. 89 (2009) 769–777.
[24] C.M. Allen, K.A.Q. O'Reilly, B. Cantor, P.V. Evans, Prog. Mater. Sci. 43 (1998) 89–170.
[25] P.R. Goulart, V.B. Lazarine, C.V. Leal, J.E. Spinelli, N. Cheung, A. Garcia, Intermetallics 17 (2009) 753–761.
[26] H.N. Thi, Y. Dabo, B. Drevet, M.D. Dupouy, D. Camel, B. Billia, J.D. Hunt, A. Chilton, J. Cryst. Growth 281 (2005) 654–668.
[27] A. Ourdjini, J. Liu, R. Elliott, Mater. Sci. Technol. 10 (1994) 312–318.
[28] E. Çardili, U. Böyük, S. Engin, H. Kaya, N. Maraslı, A. Ülgen, J. Alloys Compd. 486 (2009) 199–206.
[29] C.J. Simensen, A.I. Spjelkavik, Fresen. Z. Anal. Chem. 300 (1980) 177–182.
[30] C.J. Simensen, P. Fartum, A. Andersen, Fresen. Z. Anal. Chem. 319 (1984) 286–292.
[31] A.J. Elliott, T.M. Pollock, Metall. Mater. Trans. 38A (2007) 871–882.